

Supporting Information

Three-Dimensional Ordered Honeycomb Nanostructure Anchored with Pt-N Active Sites via Self-Assembly of Block Copolymer: An Efficient Electrocatalyst towards Oxygen Reduction Reaction in Fuel Cell

Zhida Wang^{*,1}, Yi Yang^{1,2}, Xiaoman Wang¹, Zhuoxin Lu¹, Changqing Guo¹, Yan Shi¹, Hongyi Tan¹, Lisha Shen¹, Shuo

Cao³, Changfeng Yan^{*,1,2}

¹CAS Key Laboratory of Renewable Energy, Guangdong Key Laboratory of New and Renewable Energy Research and Development, Guangzhou Institute of Energy Conversion, Chinese Academy of Sciences, Guangzhou, China, 510640.

²University of Chinese Academy of Sciences, Beijing, China, 100039.

³Institute of Metal Research, Chinese Academy of Sciences, Shenyang, China, 110016.

Email: yan cf@ms.giec.ac.cn; wang zd@ms.giec.ac.cn

1. Experimental

N-doped honeycomb nanostructure from self-assembly of Pt-loaded block copolymer. The honeycomb nanostructures with Pt (Pt/N-OHCs) were synthesized through a three-step route based on the self-assembly. Polystyrene-block-poly(4-vinylpyridine) (PS-*b*-P4VP, PDI=1.18, the molecular weights of the blocks were 40500 and 16500, respectively) was purchased from Polymer Source Inc. Quebec, Canada and used as received. Briefly, 20 mg di-BC and 10 mg phenolic resin was dissolved in 4 mL N,N-Dimethylformamide (DMF). The metal precursor of H₂PtCl₆ (Shanghai Bide Pharm Tech. Co., Ltd, 98%) was added with different weight ratios for the Pt single atoms (SAs) and ultrafine nanoparticles (NPs). Then the metal-loaded solution was dip-coated onto a silicon wafer (12×10 mm²) at a specific withdrawal rate of 2 and 5 mm/min. The coated substrates were dried in air and at room temperature for 1 day to make the micelles set on the Si wafer. Finally, the self-assembled nanopattern was heated at 400 °C in a N₂ flow for 3 h, following in Ar/H₂ flow for 2 h, and cooled down at room temperature for 48 h.

Physical characterizations. Scanning electron microscope (SEM) was conducted with an S-4800 instrument at 2.0 kV for the surface morphology observation. The film thicknesses at various dip-coating rates were measured by using a conventional method of scratches reaching the substrate surface based on atomic force microscope (AFM) technique. Morphologies identification was done through the high-resolution transmission electron microscopy (HR-TEM) and high angle annular dark-field scanning transition electron microscopy (HAADF-STEM) image on a JEM-2100 microscope. The mesoporous structure was characterized by Brunauer-Emmett-Teller (BET) method and Barrett-Joyner-Halenda (BJH) model. Raman spectra were recorded by using a 235 nm laser source. X-ray diffraction (XRD) patterns were acquired on a PANalytical X'Pert diffractometer

using Cu K α radiation. Energy-dispersive X-ray spectroscopy (EDS) characterization was used to observe the element dispersion. The point resolution was 0.23 nm and the accelerating voltage was 200 kV. X-Ray photoelectron spectroscopy (XPS) analysis was conducted through a thermo ESCALAB 250XI multifunctional imaging electron spectrometer equipped with an Al K radiation source. Inductively coupled plasma mass spectrometry (ICP-MS) analysis system was used to evaluate the elemental composition of the synthesized materials.

TEM sample preparation. The specimens on silicon wafers were transferred to a TEM copper grid by a polymer overcasting method. The metal-loaded polymer solution was spin-coated onto a silicon wafer at 1500 rpm for 60 s and dried at N₂-filled glove-box for 24 h. While the metal NPs arrays were embedded in a toluene solution of ~2 wt% polystyrene homopolymer (~M_w = 260 000 Da) and treated as same as the metal-loaded BCP solution. The silicon substrate was then immersed in concentrated HF to release the specimen film layer that contained the metal-BCP or the NP arrays. The floating layer was diluted with ~20-fold amounts of de-ionized and transferred to a TEM grid for TEM and EDS analysis, which confirmed that samples prepared by this method were similar in cluster definition and composition to those prepared directly on ITO and carbon substrates.

For the TEM of section observation, the Pt/N-OHC on the Si wafer was cut into two pieces and then spliced on the section. The backsides of the sample substrates were treated with polishing and following ion-milling and then the honeycombs on the thinned substrates were transferred to copper grids for TEM section characterization.

Electrochemical catalysis. Cyclic voltammetry (CV) and linear scanning voltammetry (LSV) tests were carried out on a tri-electrode electrochemical workstation (IviumStat.h, IVIUM

TECHNOLOGIES), with honeycomb specimens as the working electrode, a saturated silver/silver chloride electrode (Ag/AgCl, -0.2 V vs. RHE) as the reference electrode, and a Pt wire as the counter electrode. The iR-compensation was adopted in all electrochemical tests. For CV recording, the scanning range was from -0.15 to 1.0 V (vs. Ag/AgCl, namely, a range of 0.05 to 1.2 V vs. RHE) in 0.1 M N₂-saturated HClO₄ solution. The ECSA was calculated according to the formula $ECSA = Q_H / (r \cdot Q_{Href} \cdot M_{Pt})$, where r , Q_H , Q_{Href} and M_{Pt} , were the scanning rate (100 mV/s), the area of hydrogen-desorption peak, the absorbable electric quantity per cm² on Pt surface ($Q_{Href} = 0.21 \text{ mC} \cdot \text{cm}^{-2}$) and the Pt loading, respectively.

The linear scanning voltammetry (LSV) was firstly recorded in 0.1 M O₂-saturated HClO₄ aqueous solution on a rotating disk electrode system (RDE, 5 mm diameter). The rotating rate ranged from 400 to 2025 rpm and the voltage was from -0.2 to 1.0 V (vs. Ag/AgCl) at 10 mV s⁻¹. According to the LSVs, the electron transfer number were calculated by using the Koutechy–Levich (K–L) equation:[1]

$$\frac{1}{I} = \frac{1}{I_k} + \frac{1}{I_d} \quad (1)$$

where I is the current density, I_k is the kinetic limiting current density, and I_d is the diffusion-limiting current density and can be described as:[2]

$$\frac{1}{I_d} = \frac{1}{0.62nFC_0\nu^{-1/6}D_0^{2/3}\omega^{1/2}} \quad (2)$$

in which n is the electron transferred number in ORR, F is the Faraday constant (96485 C/mol), C_0 is the bulk O₂ concentration ($1.26 \times 10^{-6} \text{ mol/cm}^3$), D_0 is the is the diffusion coefficient of O₂ ($1.7 \times 10^{-5} \text{ cm}^2/\text{s}$), ν is the kinematic viscosity of the electrolyte ($1.009 \times 10^{-2} \text{ cm}^2/\text{s}$), and ω is the rotating speed. The number of transferred electrons can be calculated from the slope based on the equations (1) and (2).

The yield of hydrogen peroxide ($H_2O_2\%$) was calculated from the rotating ring-disk electrode (RRDE, E7R9, disk area: 0.25 cm^2 , Pt ring area: 0.19 cm^2) in 0.1 M O_2 -saturated $HClO_4$ solution. The scan rate was 10 mV s^{-1} and the potential of the Pt ring disk was set to 1.3 V vs. RHE. Based on the disk current (I_D) and ring current (I_R), the $H_2O_2\%$ and the electron transfer number (n) were calculated from the RRDE measurements as following:

$$H_2O_2 = \frac{2I_R}{NI_D + I_R} \quad (3)$$

$$n = \frac{4NI_D}{NI_D + I_R} \quad (4)$$

where N is the current collection efficiency of Pt ring and is equal to 0.37.

Single-cell test. Single-cell tests were performed on an ARBIN FC-100W fuel cell station (Arbin Instruments Inc.). The Pt-loaded BC solution was casted onto the carbon paper ($20\text{ mm} \times 20\text{ mm}$, HCP120, Hesen Co. Ltd.) and the following procedures were the same as described above. The cathode was prepared by using the coated carbon wafer as a membrane-electrode assembly (MEA) of a single PEMFC. The Pt loading was calculated by the dosages of the solution and verified by ICP method. For comparison, commercial Pt/C catalyst of JM 40 with Pt loading of 0.15 mg/cm^2 on cathode was used. The catalyst ink for the anode, which was prepared by mixing the JM-40 catalysts, deionized water, IPA, and Nafion ionomer, was directly coated on a Nafion 212 membrane (4 cm^2) using a spray gun. The cell temperature was set as $75\text{ }^\circ\text{C}$. 200 sccm H_2 was fed to the anode and 400 sccm O_2 was fed to the cathode with 100% relative humidity (RH). After activation, I-V polarization curves were obtained from open-circuit voltage to 0.20 V at 1.0 bar of back pressure. The ADT test was performed between 0.6 V and 0.95 V for 10000 cycles at a scan rate of 100 mV/s . The H_2 flow in the anode is 200 sccm with 100% RH and the Ar flow in the cathode is 75 sccm with 100% RH.

2. DFT Calculations

All the calculations were performed using Vienna ab initio simulation package (VASP) with the Perdew-Burke-Ernzerhof (PBE) exchange-correlation functional. The inner electrons were represented by projector augmented wave (PAW) potentials with a kinetic energy cutoff of 400 eV. The force convergence parameter was set to be 0.02 eV/Å and the Methfessel-Paxton dispersion was 0.1 eV. The free energy diagrams of ORR were calculated according to the method proposed by Nørskov and coworkers,[3] and the changes of free energy from initial to final states of the ORR could be defined as follows:[4]

$$\Delta G = \Delta E + \Delta E_{ZPE} - T\Delta S \quad (5)$$

where ΔE is the total energy change, ΔE_{ZPE} is the change of zero-point energy estimated for the adsorbed species, and ΔS is the change in entropy. Based on computational hydrogen electrode model, the chemical potential of H^+ to H_2 is calculated from:[5]

$$\mu(H^+) + \mu(e^-) = 1/2\mu(H_2(g)) - eU \quad (6)$$

The D2 method was adopted for the description of the van derWaals interactions.[6] The (5, 8, 5) graphene model with two carbon atoms replaced by nitrogen atoms was used as the N-doped structure. The k-point was set to be $3 \times 3 \times 1$. [3] The adsorption energy (E_{ad}) was calculated using the following equation:

$$E_{ad} = E_{\text{adsorbate/support}} - E_{\text{support}} - E_{\text{adborbate}} \quad (7)$$

where $E_{\text{adsorbate/support}}$, E_{support} , $E_{\text{adborbate}}$, are the total energies of the support with the adsorbate, the energy of the support, and the energy of the free adsorbate, respectively.

3. Supporting Figures

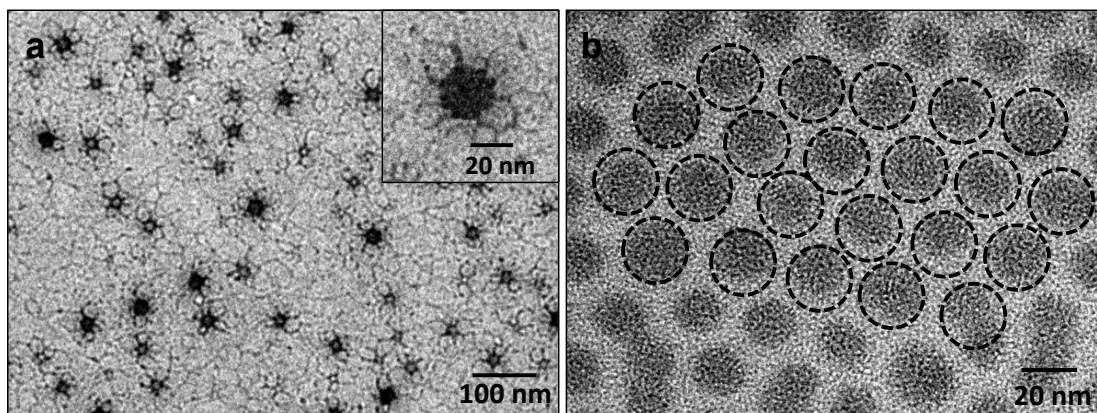


Figure S1. (a) TEM image of the Pt/BCP micellar units. (b) TEM image of the self-assembled noduled nanotemplate.

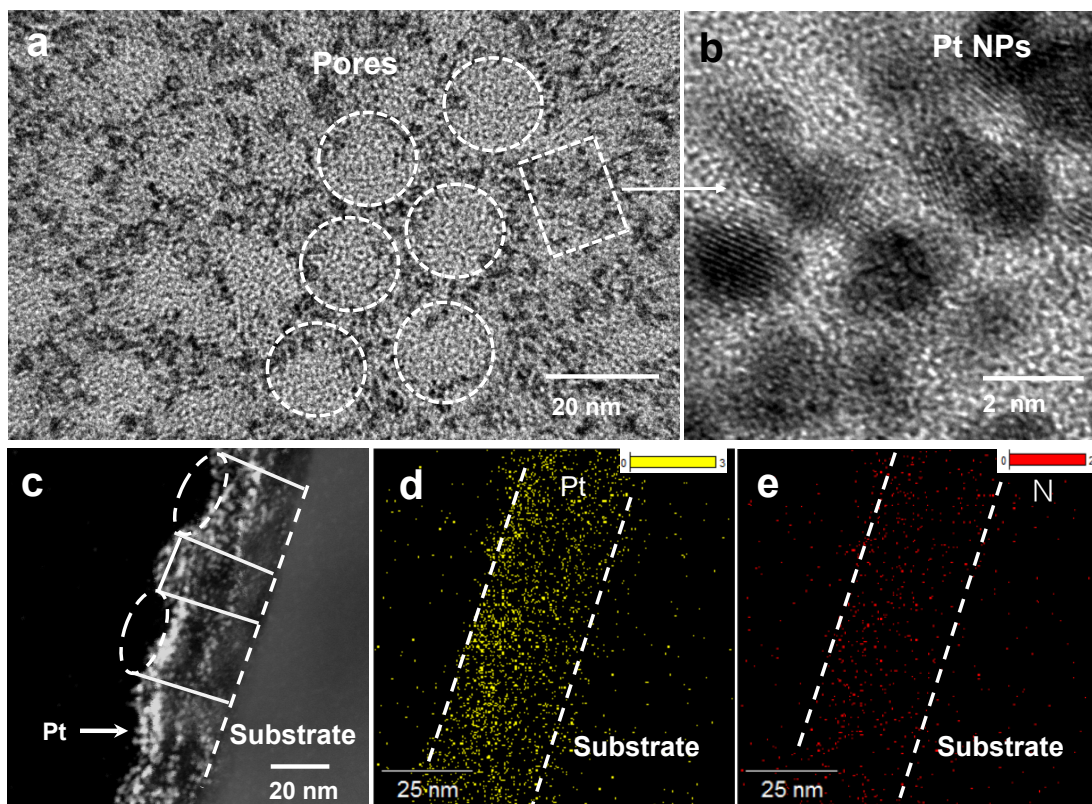


Figure S2. (a) TEM image of nPt/N-OHC. (b) Enlarged TEM picture showing ultrafine Pt NPs. (c) HAADF-STEM image of the side view of nPt/N-OHC. (d) EDS elemental mapping for Pt. (e) EDS elemental mapping for N elements.

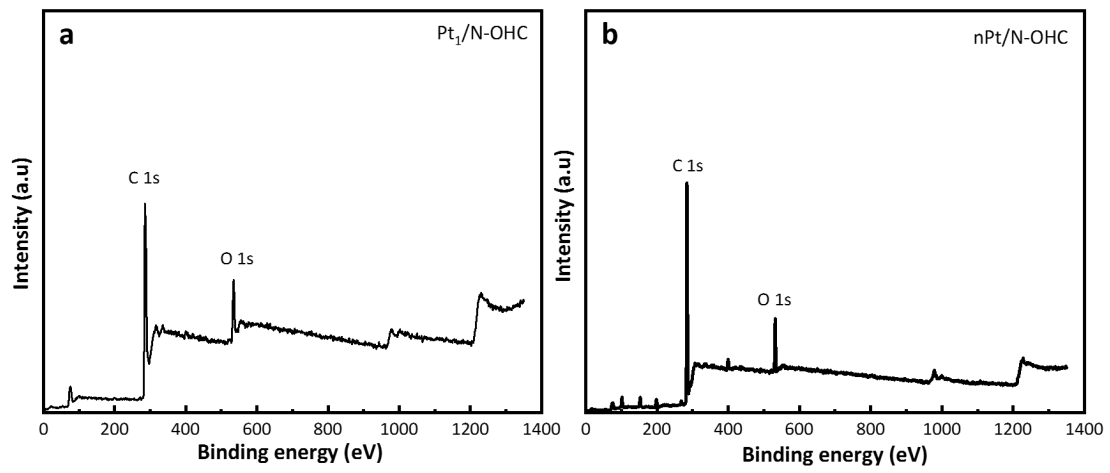


Figure S3. XPS survey for Pt/N-OHCs. (a) Pt₁/N-OHC. (b) nPt/N-OHC.

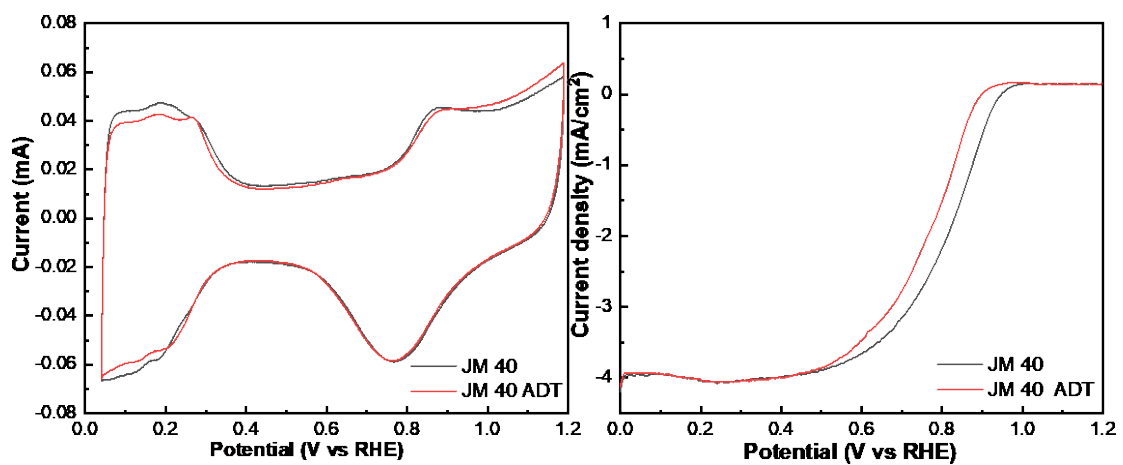


Figure S4. (a) CV curves of the commercial JM 40 Pt/C catalyst before and after ADT test. (b) LSVs of the commercial JM 40 Pt/C catalyst before and after ADT test at 1600 rpm rotating speed in 0.1 M HClO₄.

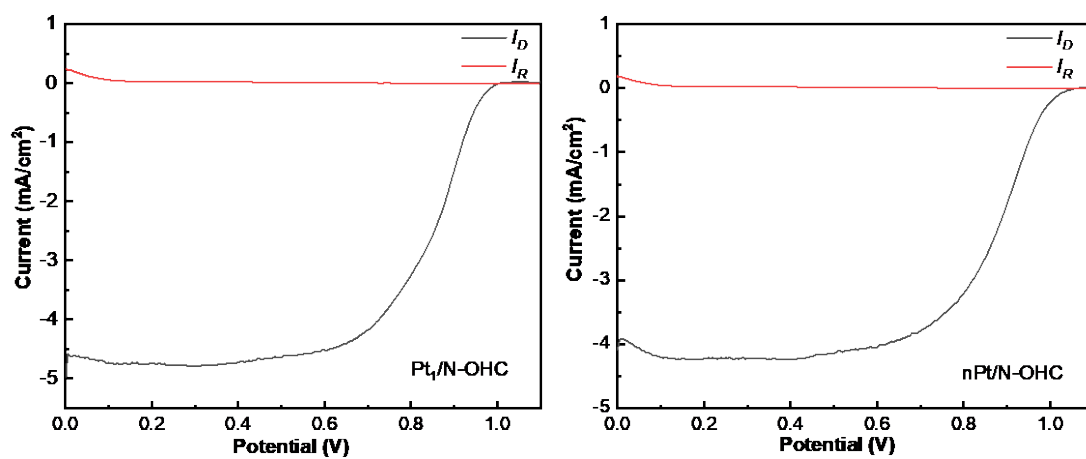


Figure S5. LSV curves derived from RRDE in O₂-saturated 0.1 M HClO₄ at 1600 rpm. (a) Pt₁/N-OHC,

(b) nPt/N-OHC.

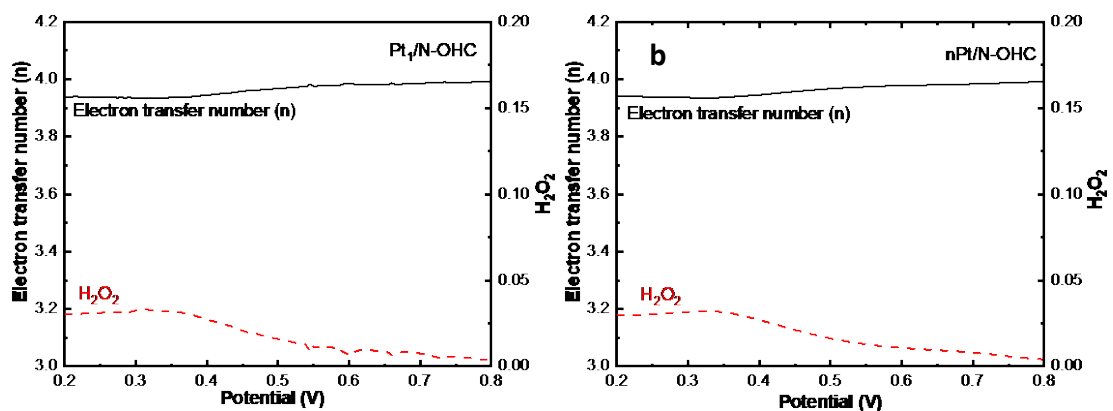


Figure S6. Electron transfer number (n) and H₂O₂ yield calculated from the RRDE measurements.

(a) Pt₁/N-OHC, (b) nPt/N-OHC.

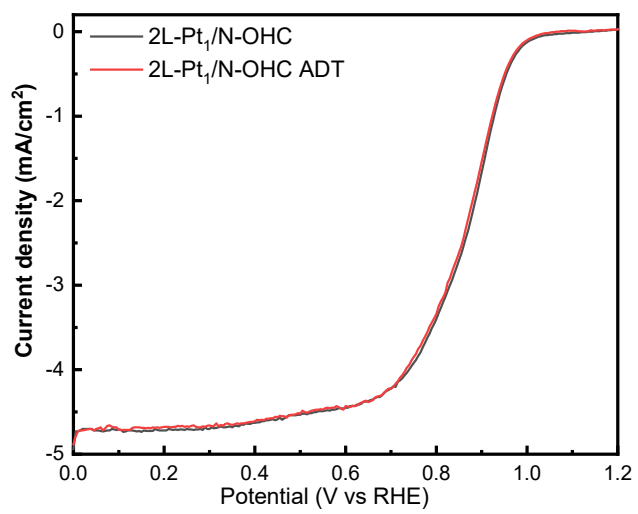


Figure S7. LSVs of the 2-layered Pt₁/N-OHC before and after ADT test at 1600 rpm rotating speed in 0.1 M HClO₄.

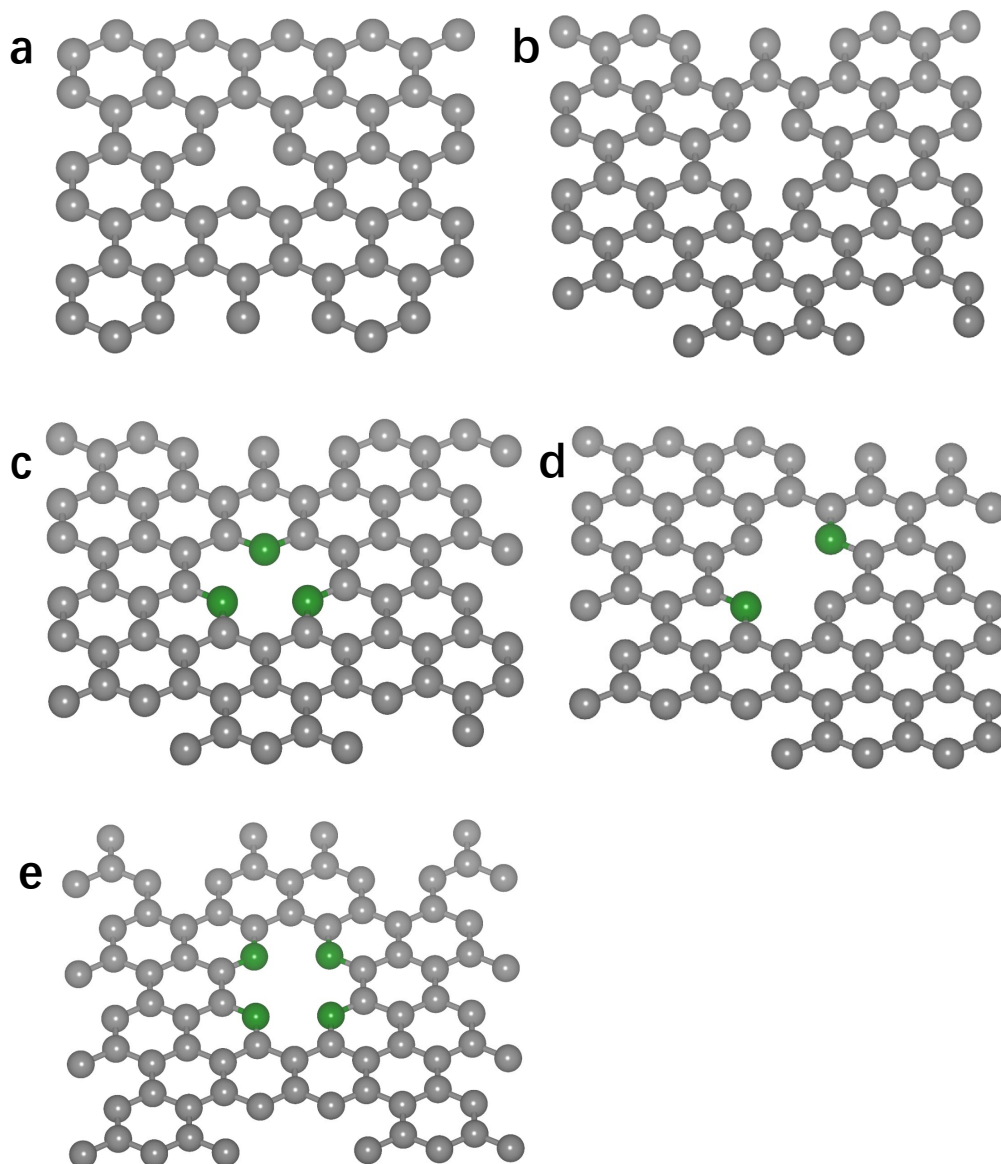


Figure S8. According to the Raman spectrum, graphene substrates with defects were considered in our case. Five optimized graphitic structures including N-doped graphene were selected. (a) gC3, (b) gC4, (c) N3-gC, (d) N2-gC, (e) N4-gC. Grey is for C and green is for N, respectively.

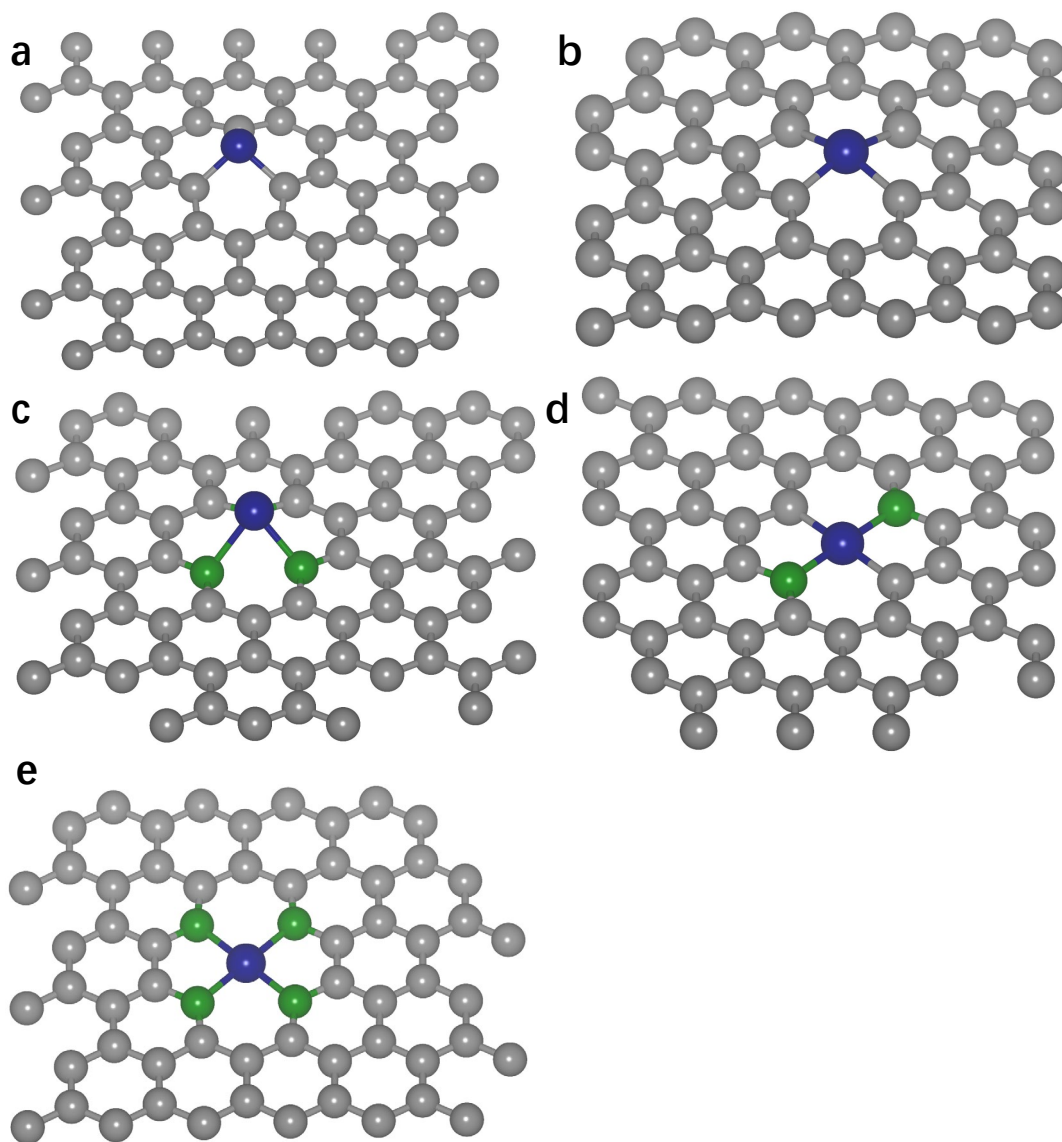


Figure S9. Optimized Pt adsorbed structure on graphitic and N-doped graphitic substrates. (a) Pt_1/gC_3 , (b) Pt_1/gC_4 , (c) $\text{Pt}_1/\text{N}_3\text{-gC}$, (d) $\text{Pt}_1/\text{N}_2\text{-gC}$, (e) $\text{Pt}_1/\text{N}_4\text{-gC}$. The grey, green, and blue colors indicate the carbon, nitrogen, and platinum, respectively.

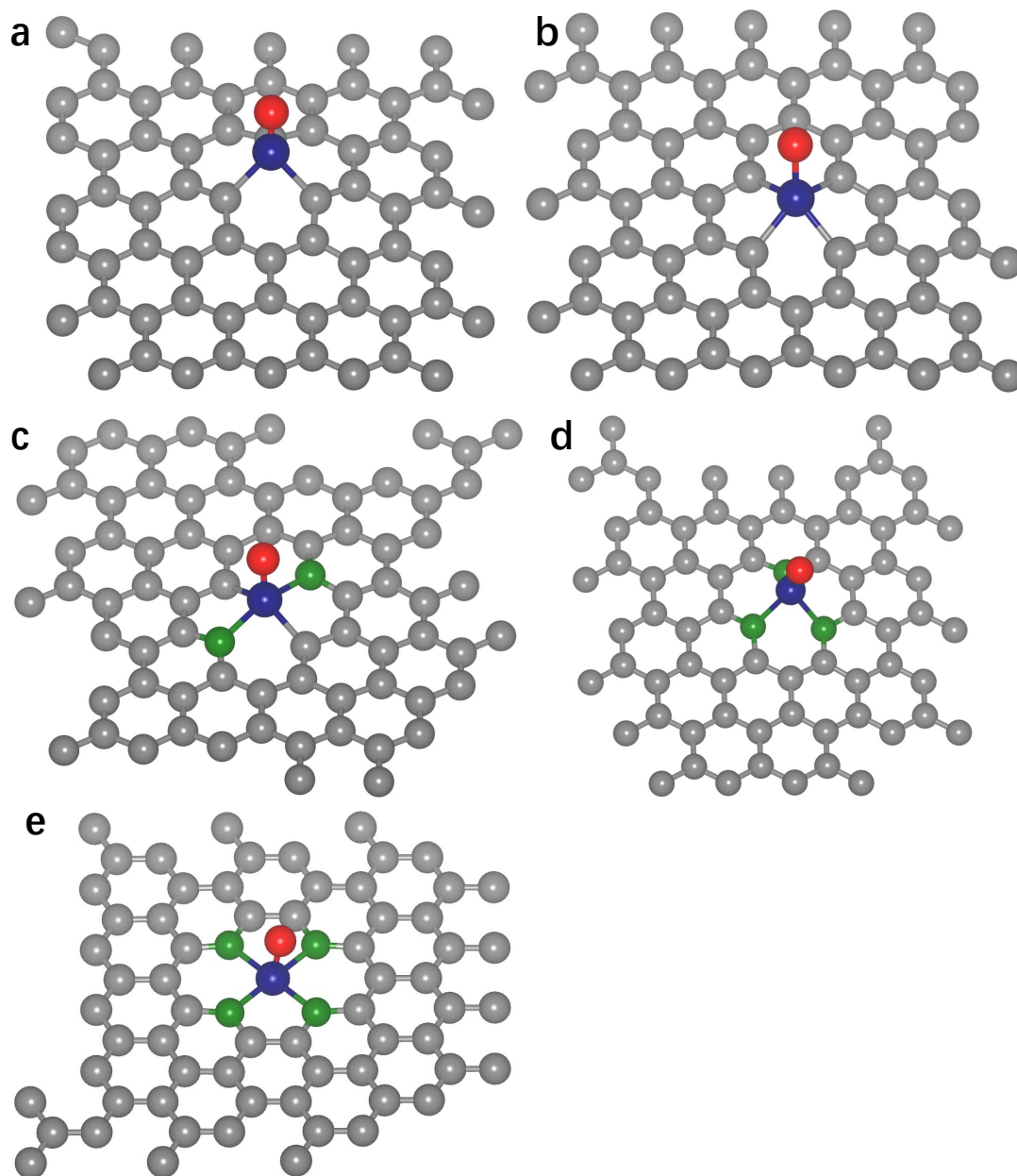


Figure S10. Optimized adsorption of O on N-doped Pt-adsorbed substrates.

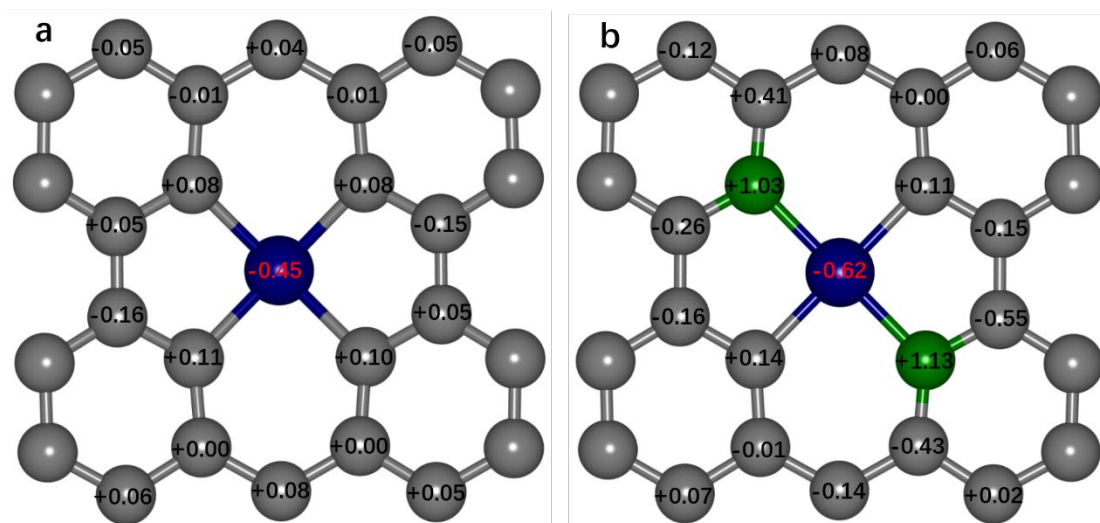


Figure S11. Bader charge analysis of (a) Pt/gC, and (b) Pt/N-gC. The more negative charge of Pt indicates that the electron transfer from Pt to N.

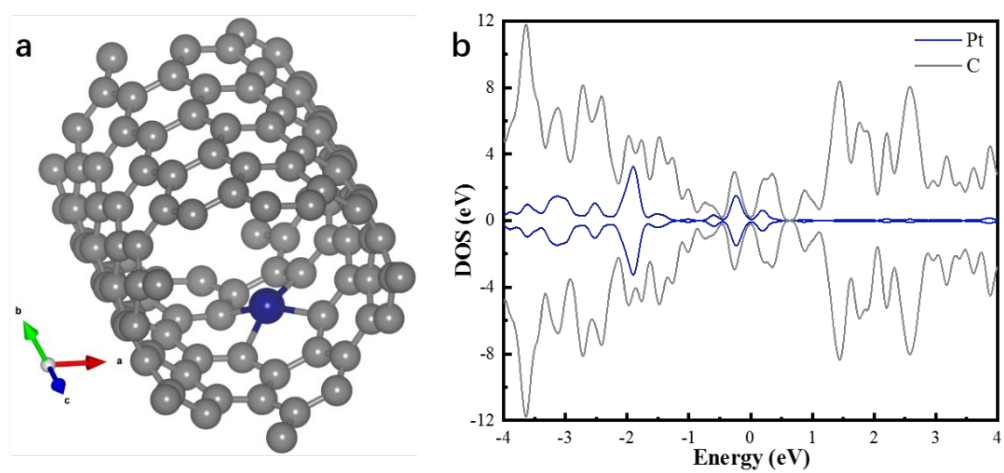


Figure S12. (a) Pt-adsorbed graphitic structure, (b) Partial DOS (in states/eV) of the Pt-adsorbed graphene.

4. Supporting Tables

Table S1. Comparison of the half-wave potentials ($E_{1/2}$) between the Pt/N-OHCs and some other typical ORR catalysts in acidic condition.

ORR catalysts	$E_{1/2}$	Electrolyte	Rotation rate (rpm)	References
Pt ₁ /N-OHC	0.88	0.1 M HClO ₄	1600	This work
nPt/N-OHC	0.86	0.1 M HClO ₄	1600	This work
2L-Pt ₁ /N-OHC	0.87	0.1 M HClO ₄	1600	This work
Pt ₁ -N/BP	0.76	0.1 M HClO ₄	1600	Ref [4]
Pt ₁ /Fe-NC	0.80	0.5 M H ₂ SO ₄	1600	Ref [7]
Pt ₁ /ZIF-C	0.88	0.1 M HClO ₄	1600	Ref [8]
Pt ₁ /NPC	0.65	0.1 M HClO ₄	1600	Ref [9]
Pt _{1.1} /BP _{defect}	0.85	0.1 M HClO ₄	1600	Ref [10]
Ir ₁ -N/C	0.83	0.1 M HClO ₄	N/A	Ref [11]
Ru ₁ /N-GC	0.89	0.1 M HClO ₄	1600	Ref [5]
Pt/NRGO	0.83	0.5 M H ₂ SO ₄	900	Ref [12]
Pt/NMC	0.75	0.1 M H ₂ SO ₄	1600	Ref [13]
Pt/TiN	0.86	0.1 M HClO ₄	1600	Ref [14]
Pt/CMC	0.87	0.1 M HClO ₄	1600	Ref [15]
Pt ₃ Co/NC	0.89	0.1 M HClO ₄	900	Ref [16]
Pt ₃ Co/ZC	0.84	0.1 M HClO ₄	1600	Ref [17]
Co ₁ /N-C	0.80	0.5 M H ₂ SO ₄	900	Ref [18]
Fe ₁ /NPS-HC	0.791	0.5 M H ₂ SO ₄	1600	Ref [19]
(Fe ₁ Co)/N-C	0.86	0.1 M HClO ₄	1600	Ref [20]

Table S2. Comparison of the Pt/N-OHCs with some other typical precious-group-metal (PGM)

based ORR electrocatalysts on MEA performance.

ORR Catalyst	Pressure (bar)	Feeding condition	PGM loading cathode/anode (mg/cm ²)	Current density at 0.6 V (A/cm ²)	Peak power density (W/cm ²)	Refs
Pt ₁ /N-OHC	1	H ₂ -O ₂	0.02/0.2	1.20	0.82	This work
nPt/N-OHC	1	H ₂ -O ₂	0.04/0.2	1.48	0.98	This work
2L-Pt ₁ /N-OHC	1	H ₂ -O ₂	0.04/0.2	1.60	1.07	This work
Pt ₁ -N/BP	0.2	H ₂ -O ₂	0.01/0.1	0.85	0.68	Ref [4]
Pt ₁ /Fe-NC	2.07	H ₂ -O ₂	0.06/0.5	1.85	0.86	Ref [7]
Pt ₁ /ZIF-C	1	H ₂ -O ₂	0.032/0.4	0.82	N/A	Ref [8]
Pt ₁ /NPC	N/A	N/A	N/A	N/A	N/A	Ref [9]
Pt _{1.1} /BP _{defect}	2	H ₂ -O ₂	0.03/0.02	0.62	0.52	Ref [10]
Ir ₁ -N/C	2	H ₂ -O ₂	0.135/0.3	1.25	0.87	Ref [11]
Ru-N/GC	N/A	N/A	N/A	N/A	N/A	Ref [5]
Pt/NRGO	N/A	N/A	N/A	N/A	N/A	Ref [12]
Pt/NMC	N/A	N/A	N/A	N/A	N/A	Ref [13]
Pt/TiN	N/A	N/A	N/A	N/A	N/A	Ref [14]
Pt/CMC	N/A	N/A	N/A	N/A	N/A	Ref [15]
Pt ₃ Co/NC	1	H ₂ -air	0.1/0.2	1.15	0.72	Ref [16]
Pt ₃ Co/ZC	1	H ₂ -O ₂	0.043/0.35	1.01	0.75	Ref [17]
Co ₁ /N-C	2.07	H ₂ -O ₂	N/0.1	0.51	0.56	Ref [18]
Fe ₁ /NPS-HC	2	H ₂ -air	N/0.15	0.31	0.333	Ref [19]
(Fe,Co)/N-C	2	H ₂ -O ₂	N/0.1	0.99	0.98	Ref [20]
PtCo@Pt/C	1.6	H ₂ -O ₂	0.15/0.2	1.51	1.05	Ref [21]
PtCo/C	1.5	H ₂ -O ₂	0.105/0.105	0.91	N/A	Ref [22]

References

- [1] P.S. Murphin Kumar, V.K. Ponnusamy, K.R. Deepthi, G. Kumar, A. Pugazhendhi, H. Abe, S. Thiripuranthagan, U. Pal, S.K. Krishnan, Controlled synthesis of Pt nanoparticle supported TiO₂ nanorods as efficient and stable electrocatalysts for the oxygen reduction reaction, *J Mater Chem A*, **2018**, *6*, 23435-23444.
- [2] Z. Li, Q. Gao, H. Zhang, W. Tian, Y. Tan, W. Qian, Z. Liu, Low content Pt nanoparticles anchored on N-doped reduced graphene oxide with high and stable electrocatalytic activity for oxygen reduction reaction, *Sci Rep*, **2017**, *7*, 43352.
- [3] J.K. Norskov, J. Rossmeisl, A. Logadottir, L. Lindqvist, J.R. Kitchin, T. Bligaard, H. Jonsson, Origin of the overpotential for oxygen reduction at a fuel-cell cathode, *J Phys Chem B*, **2004**, *108*, 17886-17892.
- [4] J. Liu, M. Jiao, L. Lu, H.M. Barkholtz, Y. Li, Y. Wang, L. Jiang, Z. Wu, D.J. Liu, L. Zhuang, C. Ma, J. Zeng, B. Zhang, D. Su, P. Song, W. Xing, W. Xu, Y. Wang, Z. Jiang, G. Sun, High performance platinum single atom electrocatalyst for oxygen reduction reaction, *Nat Commun*, **2017**, *8*, 15938.
- [5] C.H. Zhang, J.W. Sha, H.L. Fei, M.J. Liu, S. Yazdi, J.B. Zhang, Q.F. Zhong, X.L. Zou, N.Q. Zhao, H.S. Yu, Z. Jiang, E. Ringe, B.I. Yakobson, J.C. Dong, D.L. Chen, J.M. Tour, Single-Atomic Ruthenium Catalytic Sites on Nitrogen-Doped Graphene for Oxygen Reduction Reaction in Acidic Medium, *Acs Nano*, **2017**, *11*, 6930-6941.
- [6] S. Grimme, Semiempirical GGA-type density functional constructed with a long-range dispersion correction, *J Comput Chem*, **2006**, *27*, 1787-1799.
- [7] X.J. Zeng, J.L. Shui, X.F. Liu, Q.T. Liu, Y.C. Li, J.X. Shang, L.R. Zheng, R.H. Yu, Single-Atom to Single-Atom Grafting of Pt₁ onto Fe-N₄ Center: Pt₁@Fe-N-C Multifunctional Electrocatalyst with

Significantly Enhanced Properties, *Adv Energy Mater*, **2018**, *8*, 1701345.

[8] Z.X. Song, Y.N. Zhu, H.S. Liu, M.N. Banis, L. Zhang, J.J. Li, K. Doyle-Davis, R.Y. Li, T.K. Sham, L.J. Yang, A. Young, G.A. Botton, L.M. Liu, X.L. Sun, Engineering the Low Coordinated Pt Single Atom to Achieve the Superior Electrocatalytic Performance toward Oxygen Reduction, *Small*, **2020**, *16*, 2003096.

[9] T.F. Li, J.J. Liu, Y. Song, F. Wang, Photochemical Solid-Phase Synthesis of Platinum Single Atoms on Nitrogen-Doped Carbon with High Loading as Bifunctional Catalysts for Hydrogen Evolution and Oxygen Reduction Reactions, *Acs Catal*, **2018**, *8*, 8450-8458.

[10] J. Liu, M.G. Jiao, B.B. Mei, Y.X. Tong, Y.P. Li, M.B. Ruan, P. Song, G.Q. Sun, L.H. Jiang, Y. Wang, Z. Jiang, L. Gu, Z. Zhou, W.L. Xu, Carbon-Supported Divacancy-Anchored Platinum Single-Atom Electrocatalysts with Superhigh Pt Utilization for the Oxygen Reduction Reaction, *Angew Chem Int Edit*, **2019**, *58*, 1163-1167.

[11] Q.T. Liu, Y.C. Li, L.R. Zheng, J.X. Shang, X.F. Liu, R.H. Yu, J.L. Shui, Sequential Synthesis and Active-Site Coordination Principle of Precious Metal Single-Atom Catalysts for Oxygen Reduction Reaction and PEM Fuel Cells, *Adv Energy Mater*, **2020**, *10*, 2000689.

[12] J.W. Ma, A. Habrioux, Y. Luo, G. Ramos-Sanchez, L. Calvillo, G. Granozzi, P.B. Balbuena, N. Alonso-Vante, Electronic interaction between platinum nanoparticles and nitrogen-doped reduced graphene oxide: effect on the oxygen reduction reaction, *J Mater Chem A*, **2015**, *3*, 11891-11904.

[13] L. Perini, C. Durante, M. Favaro, V. Perazzolo, S. Agnoli, O. Schneider, G. Granozzi, A. Gennaro, Metal-Support Interaction in Platinum and Palladium Nanoparticles Loaded on Nitrogen-Doped Mesoporous Carbon for Oxygen Reduction Reaction, *Acs Appl Mater Inter*, **2015**, *7*, 1170-1179.

[14] S. Yang, J. Kim, Y.J. Tak, A. Soon, H. Lee, Single-Atom Catalyst of Platinum Supported on

Titanium Nitride for Selective Electrochemical Reactions, *Angew Chem Int Edit*, **2016**, *55*, 2058-2062.

[15] X. Zhao, T. Gunji, T. Kaneko, S. Takao, T. Sakata, K. Higashi, Y. Yoshida, J.J. Ge, C.P. Liu, W. Xing, J.B. Zhu, M.L. Xiao, T. Uruga, F. Tao, Z.W. Chen, Evidence for interfacial geometric interactions at metal-support interfaces and their influence on the electroactivity and stability of Pt nanoparticles, *J Mater Chem A*, **2020**, *8*, 1368-1377.

[16] X.X. Wang, S. Hwang, Y.T. Pan, K. Chen, Y.H. He, S. Karakalos, H.G. Zhang, J.S. Spendelow, D. Su, G. Wu, Ordered Pt₃Co Intermetallic Nanoparticles Derived from Metal-Organic Frameworks for Oxygen Reduction, *Nano Lett*, **2018**, *18*, 4163-4171.

[17] L. Chong, J.G. Wen, J. Kubal, F.G. Sen, J.X. Zou, J. Greeley, M. Chan, H. Barkholtz, W.J. Ding, D.J. Liu, Ultralow-loading platinum-cobalt fuel cell catalysts derived from imidazolate frameworks, *Science*, **2018**, *362*, 1276-1281.

[18] X.X. Wang, D.A. Cullen, Y.T. Pan, S. Hwang, M.Y. Wang, Z.X. Feng, J.Y. Wang, M.H. Engelhard, H.G. Zhang, Y.H. He, Y.Y. Shao, D. Su, K.L. More, J.S. Spendelow, G. Wu, Nitrogen-Coordinated Single Cobalt Atom Catalysts for Oxygen Reduction in Proton Exchange Membrane Fuel Cells, *Adv Mater*, **2018**, *30*, 1706758.

[19] Y.J. Chen, S.F. Ji, S. Zhao, W.X. Chen, J.C. Dong, W.C. Cheong, R.A. Shen, X.D. Wen, L.R. Zheng, A.I. Rykov, S.C. Cai, H.L. Tang, Z.B. Zhuang, C. Chen, Q. Peng, D.S. Wang, Y.D. Li, Enhanced oxygen reduction with single-atomic-site iron catalysts for a zinc-air battery and hydrogen-air fuel cell, *Nat Commun*, **2018**, *9*, 5422.

[20] J. Wang, Z.Q. Huang, W. Liu, C.R. Chang, H.L. Tang, Z.J. Li, W.X. Chen, C.J. Jia, T. Yao, S.Q. Wei, Y. Wu, Y.D. Lie, Design of N-Coordinated Dual-Metal Sites: A Stable and Active Pt-Free Catalyst for

Acidic Oxygen Reduction Reaction, *J Am Chem Soc*, **2017**, *139*, 17281-17284.

[21] Z.D. Wang, Y.L. Mai, Y. Yang, L.S. Shen, C.F. Yan, Highly Ordered Pt-Based Nanoparticles Directed by the Self-Assembly of Block Copolymers for the Oxygen Reduction Reaction, *Acs Appl Mater Inter*, **2021**, *13*, 38138-38146.

[22] J.R. Li, S. Sharma, X.M. Liu, Y.T. Pan, J.S. Spendelow, M.F. Chi, Y.K. Jia, P. Zhang, D.A. Cullen, Z. Xi, H.H. Lin, Z.Y. Yin, B. Shen, M. Muzzio, C. Yu, Y.S. Kim, A.A. Peterson, K.L. More, H.Y. Zhu, S.H. Sun, Hard-Magnet L1₀-CoPt Nanoparticles Advance Fuel Cell Catalysis, *Joule*, **2019**, *3*, 124-135.